

RSC Advances



This is an *Accepted Manuscript*, which has been through the Royal Society of Chemistry peer review process and has been accepted for publication.

Accepted Manuscripts are published online shortly after acceptance, before technical editing, formatting and proof reading. Using this free service, authors can make their results available to the community, in citable form, before we publish the edited article. This *Accepted Manuscript* will be replaced by the edited, formatted and paginated article as soon as this is available.

You can find more information about *Accepted Manuscripts* in the [Information for Authors](#).

Please note that technical editing may introduce minor changes to the text and/or graphics, which may alter content. The journal's standard [Terms & Conditions](#) and the [Ethical guidelines](#) still apply. In no event shall the Royal Society of Chemistry be held responsible for any errors or omissions in this *Accepted Manuscript* or any consequences arising from the use of any information it contains.

Pore formation mechanism of β nucleated polypropylene stretched membranes

Tong Wu, Ming Xiang, Ya Cao, Jian Kang, Feng Yang*

State Key Laboratory of Polymer Materials Engineering, Polymer Research Institute of Sichuan University, Chengdu 610065, People's Republic of China

*Corresponding author's e-mail address: yangfengscu@126.com; Phone: 86-28-85403118

Abstract

In this article, two β nucleated polypropylene (β -iPP) precursor films were prepared at crystallization temperatures (T_c) of 110 °C and 135 °C. The differential scanning calorimetry (DSC), wide-angle X-ray diffraction (WAXD) and scanning electron microscopy (SEM) results reveal that the two samples, which were composed of bundle-like lamellae, had similar crystallinity and particularly high content of β -crystal. However, they behaved variably when stretched at 25 °C and 90 °C. Based on the detailed characterization of morphological evolutions during stretching by 2D-WAXD and SEM measurements, a mechanism of pore formation in stretching β -iPP is presented. We found that the phase transformation of β -smectic and β - α are not the primary origin of pore formation in stretching β -iPP, instead, the micropores are directly initiated from the substantial weak interfaces between β -lamellae. Since the bundle-like β -lamella without fully developed spherulites is an asymmetric three dimensional structure, the lamellae at different angles to the tensile axis would lead to various deformational modes during stretching. Therefore, it is the polydispersity of β -lamellae in β -iPP that causes the poor pore size distribution in stretching β -iPP membrane.

Keywords: β nucleated polypropylene; pore formation; morphological evolution

1. Introduction

Since Sony's first introduction of the rechargeable lithium-ion battery in the early

1990s, many studies have been made on separators which are placed between electrodes of opposite polarity. The separator provides not only good mechanical and electrical properties but also add safety through a thermal shutdown mechanism. A novel microporous separator made from polyolefin which could provide excellent mechanical properties, chemical stability and acceptable cost has been developed and used extensively in rechargeable lithium battery^{1,2}. The most prevailing processes for making lithium-ion battery separators are “dry uniaxial stretch”³⁻⁶, “dry biaxial stretch”⁷⁻⁹ and “wet biaxial stretch”^{10, 11}. Polypropylene (PP) and Polyethylene (PE) microporous membranes obtained from these methods are available in Celgard, Ube and Asahi Kasei^{2, 7, 12, 13}. Compared with the other two methods, “dry biaxial stretch”, which is produced from nonporous iPP films with high content of β -crystals, is more economic and technologically convenient due to the free of solvents⁸. However, the separator made from “dry biaxial stretch” has large pore size and broad pore distributions, which limit its applications in high tech fields such as power battery.

Many authors have devoted to clarifying the pore formation mechanism of β -iPP during stretching^{8, 14-22}. It is well established that isotactic polypropylene (iPP) is a typical polymorphic material with several crystal modifications, i.e. the monoclinic α form, hexagonal β form and the triclinic γ form²³⁻²⁵. The α -crystal, which has a higher density (0.936 g/cm³) than β -crystal (0.921 g/cm³), is readily to transform into α -crystal during stretching at elevated temperature²⁶⁻³⁰. Shi *et al.*²¹ proposed a well accepted phase transition mechanism of pores formation in stretching β -iPP that pores originate from a volume contraction during β - α transformation. Furthermore, Chu *et al.*¹⁴⁻¹⁶ postulated a mosaic model to explain the pore formation in β -iPP. They thought that β -crystals with c axis parallel to the drawing direction are first transformed into α -crystals, and then those with c axis tilted to the drawing direction are involved in the transformation at a lower rate. Moreover, the stable β -crystals in the larger crystallites could hinder the volume shrinkage and enlarge the pores. In addition, Grant *et al.*^{17, 18, 31} optimized fabrication conditions based on annealing of the precursor films and adjustment of stretching temperature, and subsequently produced high permeability microporous membranes. They illustrated that when

β -iPP films are biaxially stretched, lamellae rotate towards the drawing direction, initial cavitation occurs between already perpendicular large β -lamellae as they separate, while smaller lamellae shear; as stretching continues, initially formed cavities develop into larger pores as lamellae further separate, less stable β -lamellae begin to transform to α phase, and stress-induced lamellar break up begins. However, Ran *et al.*¹⁹ considered that the β - α transformation could hardly be the origin of pore formation of β -iPP; instead, they proposed a defect initiation mechanism that the micropores are directly created at the weak areas or interfaces between β -lamellae and enlarge with further deformation under stress. In these previously mentioned studies, the morphological evolution during stretching were seldom presented, which is considered to be critical to understand the pore formation mechanism in stretching β -iPP membranes.

Li³²⁻³⁵ have investigated the deformation mechanism of β -iPP under tensile loading systematically, and they found that the β -phase begin to transform into α -phase once the samples are stretched to necking. In the early stage of deformation, horizontal lamellae are stretched to separation and deformation bands are formed within a spherulite. Beyond yielding, some deformation bands develop into crazes across the spherulite boundaries. The original β -spherulites are shattered due to excessive crazing and deformation bands. Lezak^{29, 30} studied the plastic deformation behavior of β -iPP in plane-strain compression at different temperatures They proposed two mechanism when deformed at room temperature, namely the inter-lamellar slip operating in the amorphous layers which would result in numerous fine deformation bands due to the crystallographic slip systems, and the cooperative kinking of lamellae which would lead to their reorientation and formation of a chevron-like lamellar arrangement. On the other hand, when deformed at elevated temperatures, shear within deformation bands leads to β - α solid state phase transformation and the newly formed α crystallites deform with an advancing strain by crystallographic slip mechanism. As a result of deformation and phase transformation within deformation bands, β -lamellae are locally destroyed and fragmented into smaller crystals.

However, more direct evidences are needed to clarify the relationship between

pore formation and lamellar deformation process of β -iPP under tensile loading. In this article, two β -iPP cast films with high contents of β -crystal were prepared at crystallization temperatures (T_c) of 110 °C and 135 °C, since several studies on crystallization of β -iPP have defined a temperature window of 105-140 °C to promote the formation of β -crystal, where the growth rate of β -crystal is faster than that of α -crystal^{36,37}. Then tensile tests were performed at different temperatures, and during these processes, a detailed characterization of morphological evolution and pore formation was conducted. Furthermore, another goal of this present article is to propose a new model to explain the mechanism of pore formation in stretching β -iPP.

2. Experimental

2.1. Materials and sample preparation

A commercially available iPP, T38F, with a melt flow rate (MFR) of 2.9 g/10 min (230 °C, 2.16 kg), $M_w = 3.8 \times 10^5$ g/mol and $M_w/M_n = 4.7$, was purchased from Petroleum Chemical Incorporation (Lanzhou, China). A highly active β -nucleating agent, NAB-83, was supplied by GCH Technology Co., Ltd (Guangzhou, China).

A master batch containing 5 wt% β -nucleating agent (NAB-83) was prepared by melt blending; then the master batch and pure iPP were extruded to produce β -iPP specimens containing 0.3 wt% NAB-83 on a twin crew extruder. The pelletized granules were subsequently extruded into β -iPP cast films through a Hapro single screw extruder (Rheometer 200C) fitted with a slit die of 0.5 mm \times 100 mm (thickness \times width) and a three-roll calender. The extrusion was carried out at 220 °C. To promote the formation of β -crystal, the extruded film cooling rate and the crystallization behavior was controlled. The distance between the die exit and the chill roll was about 5 mm and draw ratio of 6 was applied. Two cast films were extruded with a chill roll operated at temperatures of 110 °C (PP-110) and 135 °C (PP-135). Melt flow rates and roll take-up speeds were controlled so that nominal film thicknesses of 0.2 mm and consistent crystallization conditions upon film cooling were achieved.

Uniaxial stretching of these resultant β -iPP cast films was performed using an MTS

Universal tensile testing machine equipped with a temperature chamber. The samples were uniaxially stretched to a predetermined strain (ϵ) = 100%-500% at 25 °C and 90 °C with a constant cross-head speed of 10 mm/min. A sequential biaxial stretching was performed to obtain porous membranes, comprising the longitudinally stretching (MD) to 300% at 90 °C and then transversely stretching (TD) to 300% at 115 °C^{7, 8, 13}. The samples stretched to predetermined strains were quenched by ultralow temperature solution in the stretched state in order to freeze the structural characteristics achieved. The samples were then stored in liquid nitrogen before further analysis.

2.2. Measurements

2.2.1 Differential scanning calorimetry (DSC)

All the calorimetric experiments were carried out using a Mettler Toledo DSC1 differential scanning calorimeter (DSC) under nitrogen atmosphere (50 mL/min). Calibration for the temperature scale was performed using indium as a standard to ensure reliability of the data obtained. 5 mg round samples were punched out the cast films and heated from 25 °C to 190 °C at a rate of 10 °C/min. The melting temperature (T_m) of the cast film was determined from the heating curve. The crystallinity ($X_{c,dsc}$) of the sample was calculated from the commonly used equation: $X_{c,dsc}\% = \Delta H_{exp} / \Delta H_{id} \times 100$ where ΔH_{exp} and ΔH_{id} are the experimentally measured melting enthalpy and that of the 100% crystalline sample, respectively. The values of α -modifications $\Delta H_{id}^\alpha = 177.0$ J/g and β -modifications $\Delta H_{id}^\beta = 168.5$ J/g were taken³⁷. The fraction of β phase ($K_{\beta,DSC}$) can be calculated from the following equation:

$$K_{\beta, DSC}(\%) = \frac{X_{c\beta}(\%)}{X_{c\alpha}(\%) + X_{c\beta}(\%)} \times 100\% \quad (1)$$

where $X_{c\alpha}(\%)$ and $X_{c\beta}(\%)$ are the degrees of crystallinity for α phase and β phase, respectively.

2.2.2 Two-dimensional wide-angle X-ray diffraction (2D-WAXD)

The crystalline structures of samples were investigated using DX-1000 diffractometer. The wavelength of CuK α was $\lambda=0.154$ nm and the spectra were

recorded in the 2θ range of $5\text{--}35^\circ$, a scanning rate of $2^\circ/\text{min}$, and a scanning step of 0.02° . 1D-WAXD profiles were obtained from circularly integrated intensities of the 2D-WAXD patterns acquired. The relative amount of the β phase, $K_{\beta, \text{XRD}}$, was evaluated according to Turner-Jones et al.²³

$$K_{\beta, \text{XRD}} = \frac{A_{\beta(300)}}{A_{\alpha(110)} + A_{\alpha(040)} + A_{\alpha(130)} + A_{\beta(300)}} \quad (2)$$

where $A_{\beta(300)}$ is the area of the (300) reflection peak of β phase at $2\theta = 16.1^\circ$; $A_{\alpha(110)}$, $A_{\alpha(040)}$, and $A_{\alpha(130)}$ are the areas of the (110), (040), and (130) reflection peaks of the α phase and correspond to $2\theta = 14.1^\circ$, 16.9° , and 18.6° , respectively.

The overall crystallinity, $X_{c, \text{xrd}}$, was calculated according to the following equation^{38, 39}:

$$X_{c, \text{xrd}} = \frac{\sum A_{\text{cryst}}}{\sum A_{\text{cryst}} + \sum A_{\text{amorp}}} \quad (3)$$

where A_{cryst} and A_{amorp} are the fitted areas of crystal and amorphous region, respectively.

2.2.3 Scanning electron microscopy (SEM)

The SEM experiments were performed using a Hitachi S3400tEDX SEM instrument to inspect the crystalline structure changes of films etched by a mixed acid solution⁴⁰. The samples were gold-coated and observed under an acceleration voltage of 5 kV.

2.2.4 Porosity determination

The porosity of the membranes is defined as their volume content of pores and was determined according to the following equation^{19, 22}:

$$\text{Porosity} = V_p/V_f = (V_f - V_r)/V_f \quad (4)$$

where V_f is the gross volume of the film specimen which consists of two parts, the volume occupied by the polymer resin V_r , and the volume occupied by the pores V_p . V_f was obtained from direct size measurement of the specimens. V_r was derived from the weight of the specimen and the average density of the polymer regions in the specimen, the latter can be determined according to the crystallinity of the specimen. For each sample, the average value reported was derived from at least five specimens.

As supplementary, the porosity was also measured through the following procedures: the stretched sample was immersed in ethanol for 24 h, after that, the sample was taken out and the ethanol on the surface was carefully removed using filter paper. Finally, the treated sample was weighted carefully. The porosity was calculated according to the following relation:¹¹

$$\text{Porosity} = \frac{(W_0 - W)\bar{\rho}}{\rho W_0 - (\rho - \bar{\rho})W} \times 100\% \quad (5)$$

where W is the initial sample weight, W_0 is the immersed sample weight. ρ (0.8 g/cm³) and $\bar{\rho}$ (0.91 g/cm³) are the density of ethanol and PP, respectively.

3. Results and discussion

3.1. Characterization of cast films

Thermal and X-ray techniques were employed to provide insight about the populations of crystals in these β -iPP precursor films, and several key properties arising from the crystallinity are presented in Table 1. Due to the melt-recrystallization that occurs in β -iPP during the heating DSC scan, the calculated crystallinity and fraction of β crystal may not be reliable. Thus, it is more practical to use WAXD measurement to track these properties individually. The WAXD spectra of the two β -iPP cast films are shown in Fig. 1a. It is clear to see that both samples exhibited the characteristic diffraction peak at $2\theta = 16.1^\circ$, which corresponds to the (3 0 0) crystal plane of β phase; meanwhile, no α crystal diffraction peaks of $\alpha(1\ 1\ 0)$, $\alpha(0\ 4\ 0)$, and $\alpha(1\ 3\ 0)$ were detectable, indicating that both samples are composed of almost pure β phase^{36, 41-44}. Furthermore, their crystallinity that were calculated from WAXD and DSC measurements, $X_{c,XRD}$ and $X_{c,DSC}$, were nearly the same (listed in Table 1). However, their thermodynamic behaviors in DSC test differed considerably. Heat flow curves measured during first heating scans of the precursor films (shown in Fig. 1b) reveal different melting peaks for β and α endotherms. Since the WAXD results have proven that the β crystal contents ($K_{\beta,XRD}$) of both samples were higher than 99.0%, the melting peaks of α -crystals were likely due to the

melting-recrystallization of unstable β crystal. The sample PP-110 displayed double β peaks, seen in the form of β_1 and β_2 endotherms, are typical of polymorphic β -iPP, resulting from the instability of the β_1 crystals formed at high cooling rates and propensity to recrystallize to β_2 ^{37, 45-47}, while the sample PP-135 exhibited only one β peak. Furthermore, the $K_{\beta, DSC}$, obtained from DSC, increased dramatically from 69.2% (PP-110) to 91.0% (PP-135), which further corroborates that the β crystal formed at $T_c = 110^\circ\text{C}$ was less stable than those obtained at $T_c = 135^\circ\text{C}$. Additionally, the melting peak temperature of β crystal ($T_{m, \beta 1}$) ascended from 143.6°C (PP-110) to 153.1°C (PP-135), indicating that the β -lamellar thickness increased with elevating T_c .

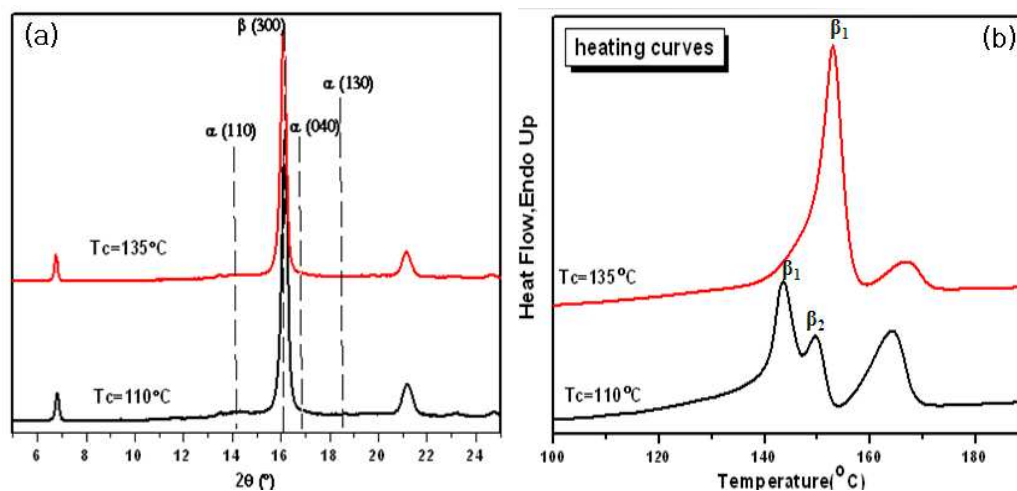


Fig. 1. (a) WAXD and (b) DSC spectra of the β -iPP samples crystallizing at 110°C and 135°C , respectively.

Table 1 The morphological characteristics of the β -PP samples crystallizing at 110°C and 135°C , respectively.

Samples	$X_{c, DSC}(\%)^a$	$X_{c, XRD}(\%)^b$	$T_{m, \beta 1}(\text{C})^a$	$K_{\beta, DSC}(\%)^a$	$K_{\beta, XRD}(\%)^b$
$T_c = 110^\circ\text{C}$	46.8	56.2	143.6	69.2	>99.0
$T_c = 135^\circ\text{C}$	48.6	57.1	153.1	91.0	>99.0

^a Crystallinity and melting temperature were measured by DSC.

^b Crystallinity and the relative amount of the β phase were calculated by WAXD.

In order to provide direct observation of their spherulitic structures, the

micrographs of the two β -iPP samples after etched were examined by SEM (shown in Fig. 2). It is interesting to see that both samples were mainly composed of bundle-like lamellae without fully developed spherulite, which is quite different from the cross-hatched structure of α -spherulite. This peculiar structure increases the tendency for β -iPP to cavitate during stretching^{37, 48}. Furthermore, the β -lamellae formed at $T_c = 135$ °C (approximate 35nm) was thicker than those formed at $T_c = 110$ °C (about 26nm).

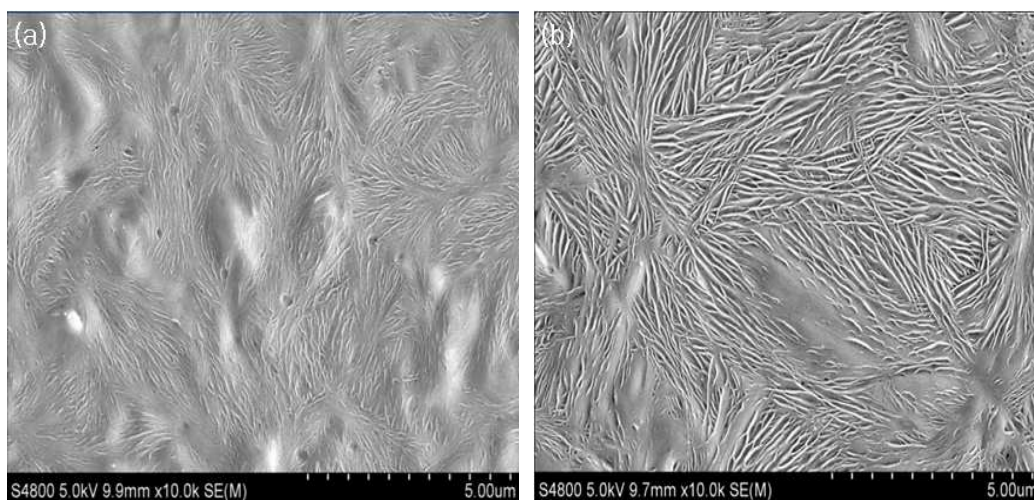
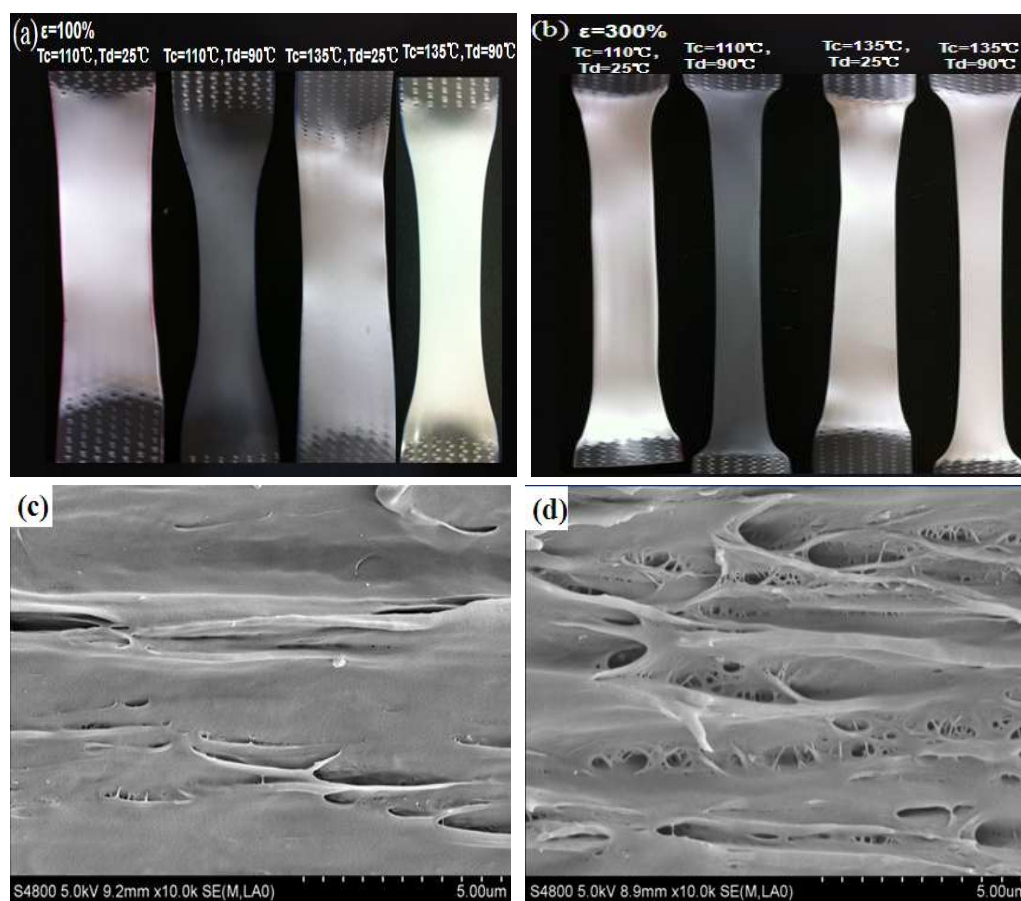


Fig. 2. SEM images of the β -PP samples after etched: (a) PP-110 and (b) PP-135.

3.2. Morphological characterization of stretched PP membranes

The photographs of uniaxially stretched β -iPP membranes at different temperatures are shown in Fig. 3a and b. It is very interesting to see that a typical necking was observed for both samples of M-PP-110 and M-PP-135 (“M” is used to designate stretched membranes) when stretched at the drawn temperature (T_d) of 90 °C, while a more homogeneous deformation was developed when stretched at 25 °C. More interestingly, the M-PP-110 sample was almost transparent at any strains when stretched at 90 °C, implying that few pores formed in these processes. On the contrary, the deformed region of M-PP-135 was completely opaque at $T_d=90$ °C, indicating that abundant microvoids might have formed in the membrane. Furthermore, the porosity results of β -iPP membranes stretched at different temperatures are also listed in Table 2. First of all, it is interesting to note that compared with those stretched at 25 °C, the

porosity of M-PP-110 decreased significantly when stretched at 90 °C, and a slight decline of porosity was also observed for M-PP-135 at $T_d=90$ °C. More importantly, M-PP-110 exhibited the highest porosity (20.3%) at $\epsilon=200\%$ when stretched at 25 °C, while M-PP-135 reached a maximum (23.1%) at $\epsilon=300\%$. On the other hand, cross section images of biaxially stretched membranes (shown in Fig. 3c and d) disclose that few pores were formed in M-PP-110, while numerous pores were originated in M-PP-135, which is in good agreement with the results of porosity in Table 2. Moreover, the surface images (shown in Fig. 3e and f) exhibit that the pore size distribution of both membranes were very poor.



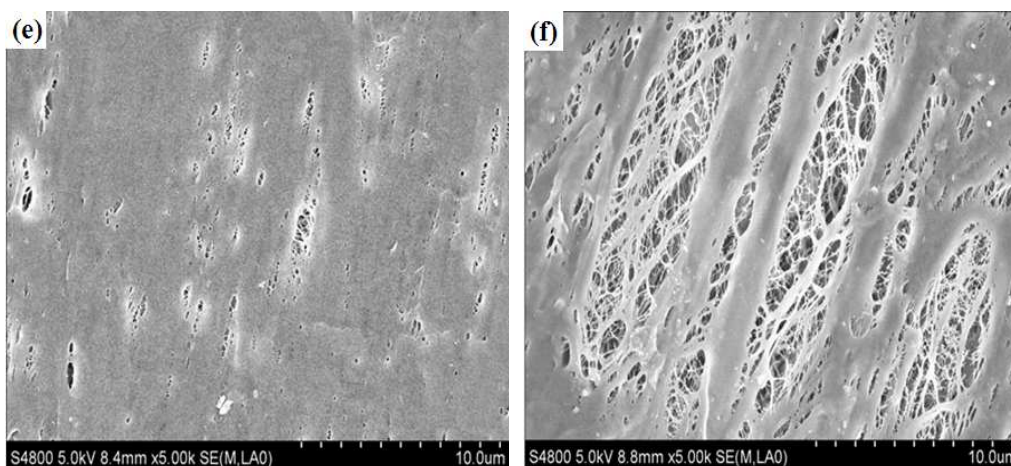


Fig. 3. Photographs of β -PP membranes after uniaxially stretched to different strains at 25 °C and 90 °C: (a) 100% and (b) 300%; cross section images of biaxially stretched membranes with free width: (c) M-PP-110 and (d) M-PP-135, 10000 \times ; and surface images: (e) M-PP-110 and (f) M-PP-135, 5000 \times .

Table 2 Porosity estimation of β -PP membranes stretched to different strains with free width at 25 °C and 90 °C, the standard deviation is $\pm 5\%$.

Samples	$T_d=25\text{ }^\circ\text{C}$ (%)				$T_d=90\text{ }^\circ\text{C}$ (%)				$T_{d,MD}=90\text{ }^\circ\text{C}$, $T_{d,TD}=115\text{ }^\circ\text{C}$ (%)
	100%	200%	300%	400%	100%	200%	300%	400%	300% \times 300%
PP-110	11.8	20.3	19.8	15.3	5.5	4.3	3.2	3.0	10.2
PP-135	9.7	19.5	23.1	19.4	9.0	17.6	21.3	18.5	45.1

Why did the precursor films of PP-110 and PP-135, which had almost the same contents of β -crystals and similar crystallinity, behaved diversely when stretched at different temperatures? Why was the pore size distribution in these membranes so poor? Microscopic lamellar evolutions and phase transitions of β -iPP during stretching will be further discussed in the following sections.

3.3. 2D-WAXD analysis of stretched PP membranes

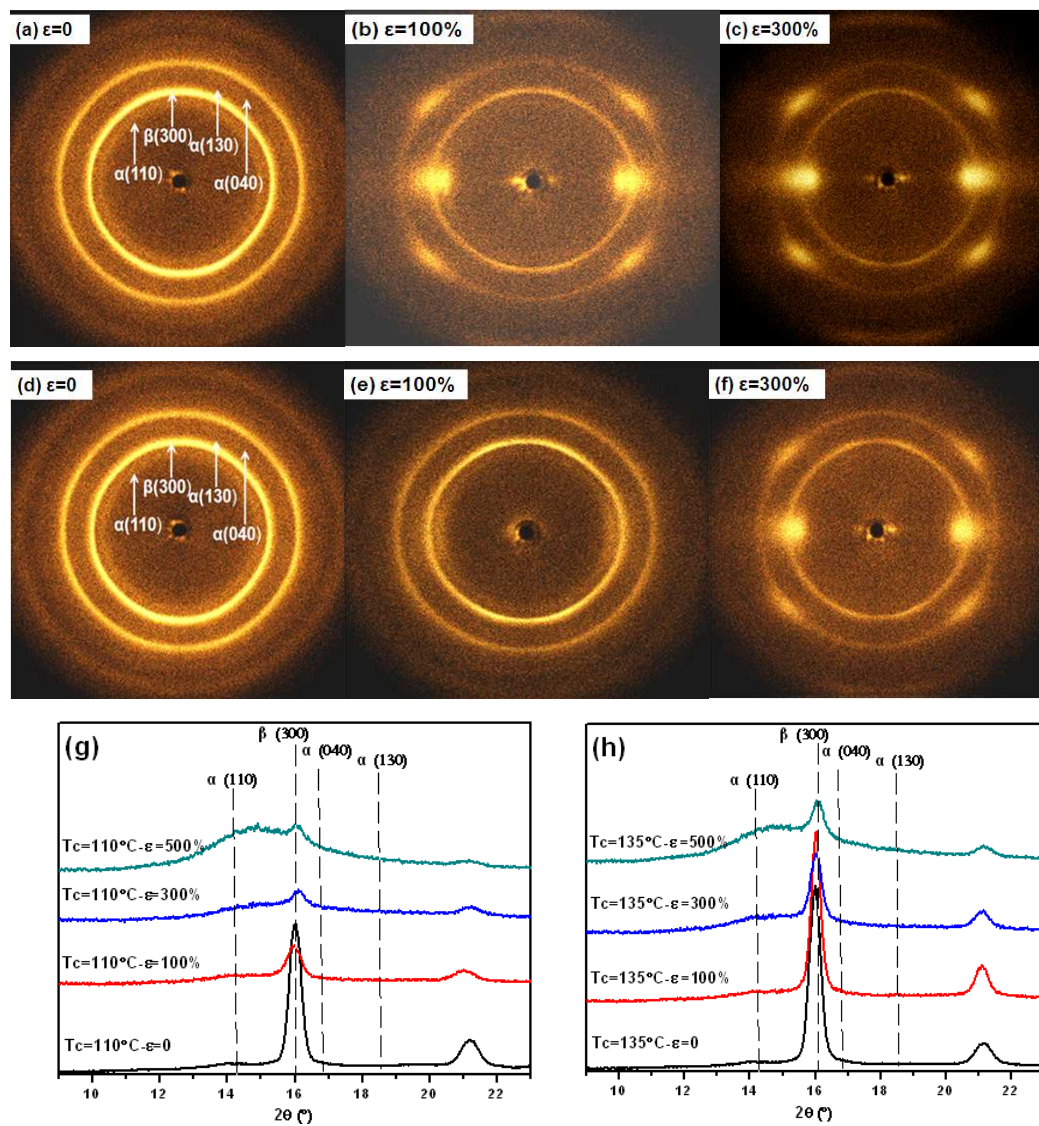
3.3.1 Stretching at 25 °C

The 2D-WAXD measurements were carried out to detect the phase transitions of β -iPP at several stages of deformation at 25 °C and 90 °C. Fig. 4 shows the diffraction

patterns of PP-110 and PP-135 samples stretching at 25 °C. First of all, it should be noted that both the cast films of β -iPP crystallizing at 110 °C and 135 °C (shown in Fig. 4a and d) exhibited the same diffraction patterns, namely the strong diffraction intensity of β (3 0 0) plane without obvious diffraction peaks of α (1 1 0), α (0 4 0), and α (1 3 0) planes, indicating that both samples are composed of almost pure β -crystals. For the sample of PP-110, the reflection of β (3 0 0) weakened significantly with a concomitant broad peak on the equator with increasing strains (seen in Fig. 4b and c). These broad and diffuse peaks are often regarded as the fingerprint of metastable smectic phase of β -iPP^{23, 36, 37, 41}. However, the PP-135 still had a strong intensity of β (3 0 0) plane with a weak diffuse reflection on the equator at $\epsilon=100\%$ (seen in Fig. 4e and f), suggesting that the β -lamellae of PP-135 are more stable than those in PP-110 during stretching. The 1D-WAXD intensity profiles of PP-110 and PP-135 as a function of strains at $T_d=25\text{ }^\circ\text{C}$ are also presented in Fig. 4g and h, respectively. As the strain increased, the diffraction intensity of β (3 0 0) plane weakened gradually with a concomitant appearance of the diffuse reflection ($2\theta = 13\text{-}20^\circ$), which corroborates that β phase transformed into c-axis oriented smectic phase when stretched at 25 °C^{19, 21, 49}. Furthermore, the β (3 0 0) intensity of PP-110 decreased more rapidly than that of PP-135 with increasing strains, which suggests that the β -lamellae formed at $T_c=135\text{ }^\circ\text{C}$ were more stable than those formed at $T_c=110\text{ }^\circ\text{C}$.

Furthermore, it is also worth mentioning that an intact β (3 0 0) ring was observed during the whole stages of deformation for both β -iPP samples, implying that the chains orientation of β -lamellae was almost unchanged during stretching. The azimuthal intensity of β (3 0 0) reflection peaks during stretching, which could characterize the β crystal phase orientation along and across the loading direction, are presented in Fig. 4i and j. The corresponding diffraction maxima are indicated as $\beta_{//}$ and β_{\perp} . For PP-110 when stretched to 100% at 25 °C, the azimuthal intensity of β_{\perp} was higher than that of $\beta_{//}$, implying that at early stage of deformation, the β -lamellae parallel to the stretching direction are much easier to fragment than those perpendicular to stretching direction. As the strain increased to 300%, the azimuthal

intensity of β_{\parallel} shifted towards a higher value than that of β_{\perp} , which indicates that fragmented β -lamellae have transformed into c-axis oriented smectic phase substantially. However, as for PP-135 stretched at 25 °C, the azimuthal intensity maxima of β_{\parallel} appeared when the strain reached 300% and was much lower than that of β_{\perp} , suggesting that the β phase formed at $T_c = 135$ °C was more stable and could resist the deformation effectively.



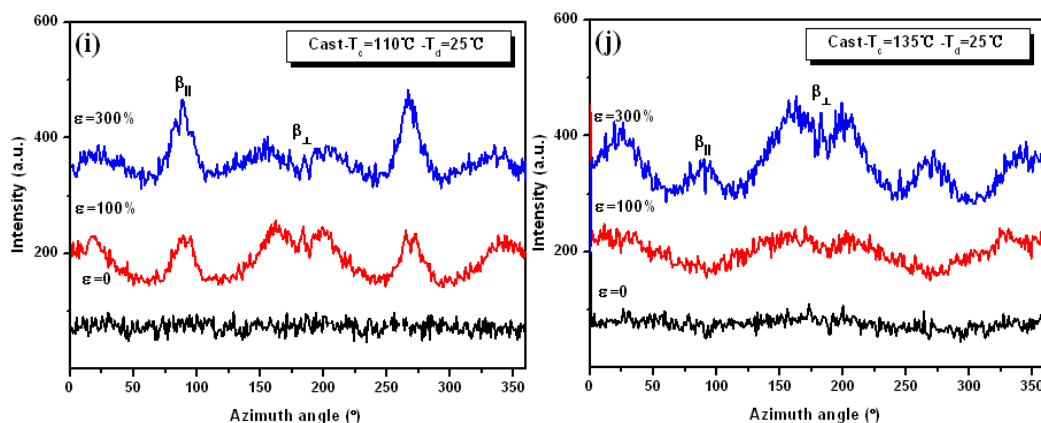


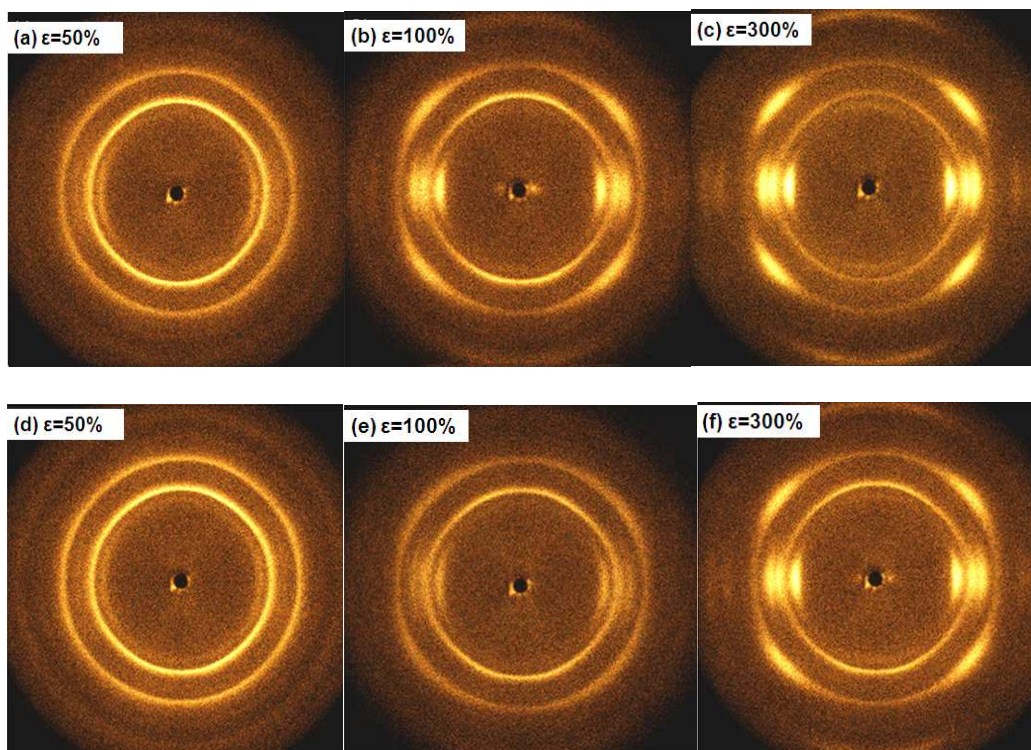
Fig. 4. 2D-WAXD patterns and corresponding 1D-WAXD profiles of β -PP membranes in terms of strain at 25 °C: (a) PP-110; (b) M-PP-110, $\varepsilon = 100\%$; (c) M-PP-110, $\varepsilon = 300\%$; (d) PP-135; (e) M-PP-135, $\varepsilon = 100\%$; (f) M-PP-135, $\varepsilon = 300\%$; (g) 1D-WAXD profile of M-PP-110; (h) 1D-WAXD profile of M-PP-135; azimuthal intensity of β (3 0 0) reflection peaks during stretching at 25 °C: (i) M-PP-110 and (j) M-PP-135. The stretching direction is horizontal.

3.3.2 Stretching at 90 °C

The 2D-WAXD patterns of PP-110 and PP-135 samples stretching at $T_d = 90$ °C are shown in Fig. 5a-f. It is clear to see that three arcs corresponding to α (1 1 0), α (0 4 0) and α (1 3 0) reflections appeared in the equator for both PP-110 and PP-135 samples when the strain was higher than 50%, which indicates that the β - α transformation enters into action at $T_d = 90$ °C^{14-16, 19, 21}. It has been widely accepted that the molecular chains of α -crystal arrange in alternating right-handed and left-handed chain layers, while the β -crystal has the same directional helical chains, thus the change of packing pattern from hexagonal to monoclinic cannot be achieved by simple adjustment of the relative positions of the neighbouring chains through slipping at low temperature but involves the destruction (melting) of the original β -crystal and rearrangement (recrystallization) of the chains to form new α -crystal at high temperature^{14-16, 19, 29, 30, 37}. On the other hand, the 1D-WAXD intensity profiles (shown in Fig. 5g and h) and the relative contents of the residual β -crystal in β -iPP membranes (listed in Table 3) reveal that the β - α transformation, which started

beyond the yield point ($\epsilon=20\%$), proceeded gradually with the increasing strains. Furthermore, this phase transformation process developed more quickly for the PP-110 than for PP-135, indicating that β -crystals formed at 110°C were less stable than those formed at 135°C , which is in accord with the trend at $T_d=25^\circ\text{C}$.

The azimuthal intensity of β (3 0 0) reflection peaks, when stretched at 90°C (shown in Fig. 5i and j), were quite different from those in Fig. 4i and j. The $\beta_{//}$ intensity of both samples maintained the minima during the whole deformation processes at $T_d=90^\circ\text{C}$, while the azimuthal intensity of β_{\perp} ascended gradually with increasing strains, which implies that the β -crystals parallel to the tensile axis were much easier to deform than those at a tilt angle to the tensile axis. Since the β - α transformation was activated when $T_d>80^\circ\text{C}^{14-16, 29, 30, 37}$, these fragments of β -crystals would transform into α -crystals immediately, thus leading to the rapid decline of the $\beta_{//}$ azimuthal intensity.



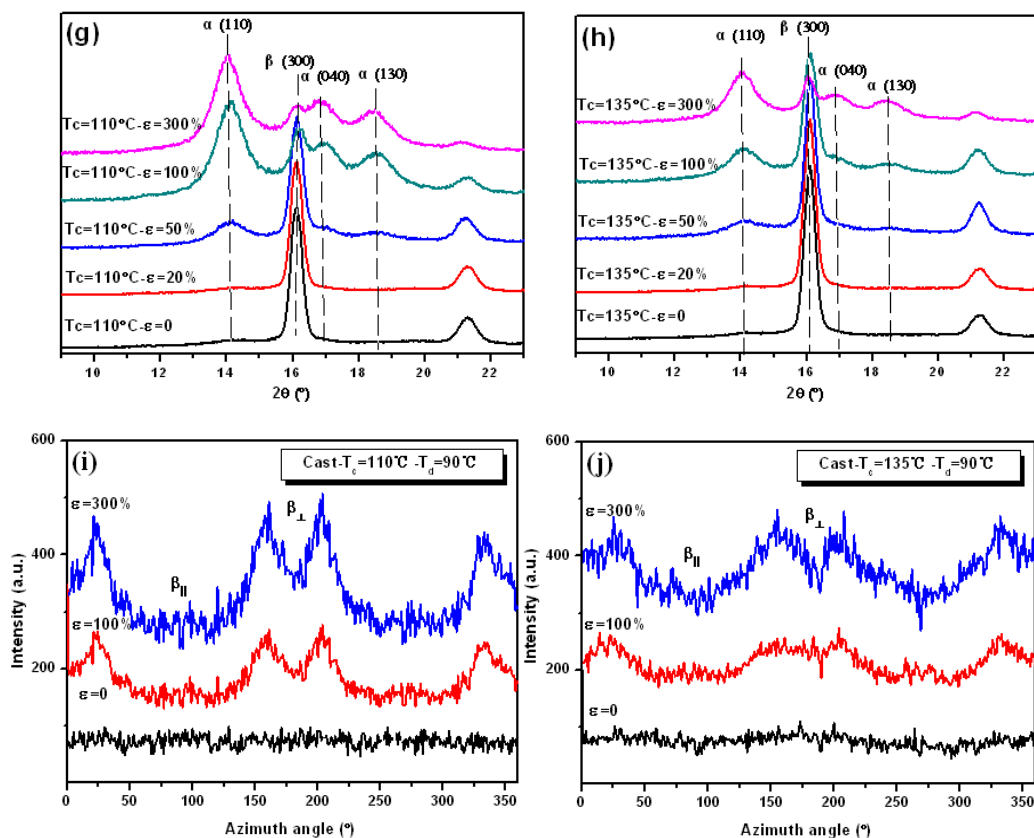


Fig. 5. 2D-WAXD patterns and corresponding 1D-WAXD profiles for β -PP membranes in terms of strains at 90°C : (a) M-PP-110, $\varepsilon = 50\%$; (b) M-PP-110, $\varepsilon = 100\%$; (c) M-PP-110, $\varepsilon = 300\%$; (d) M-PP-135, $\varepsilon = 50\%$; (e) M-PP-135, $\varepsilon = 100\%$; (f) M-PP-135, $\varepsilon = 300\%$; (g) 1D-WAXD profile of M-PP-110; (h) 1D-WAXD profile of M-PP-135, azimuthal intensity of β (3 0 0) reflection peaks during stretching at 90°C : (i) M-PP-110 and (j) M-PP-135. The stretching direction is horizontal.

Table 3 The relative amount of the β -crystal, K_β , as a function of strains for PP-110 and PP-135 at $T_d=90^\circ\text{C}$.

Strains	PP-110 (%)	PP-135 (%)
$\varepsilon = 0$	>99.0	>99.0
$\varepsilon = 20\%$	>99.0	>99.0
$\varepsilon = 50\%$	80.1	97.5
$\varepsilon = 100\%$	47.5	81.0
$\varepsilon = 300\%$	5.9	15.0

Together with the porosity results listed in Table 2, it is very interesting to note that stretching at 25°C , in which β -smectic phase transformation was predominant,

induced even a higher porosity than stretching at 90 °C, in which β - α phase transformation was activated. Furthermore, a large number of microvoids had formed at even low strain without substantial phase transformation of β -smectic or β - α . On the other hand, although PP-110 underwent a more rapid β - α transformation compared with PP-135 when stretched at 90 °C, it had a much lower porosity. These results strongly suggest that the phase transformation could hardly be the primary origin of pore formation in stretching β -iPP membrane. The phase transition and the pore formation might be two independent processes under tensile loading. In order to further understand the mechanism of pore formation in β -iPP, the detailed microscopic lamellar deformation processes during stretching will be discussed below.

3.4. SEM examination of stretched β -iPP membranes

3.4.1 Stretching at 25 °C

Fig. 6 shows the SEM micrographs of PP-110 and PP-135 at yielding point ($\epsilon = 20\%$) when stretched at 25 °C. It is clear to see that a great number of deformation bands, which were perpendicular to the tensile axis, had been originated, since the tie chains are less abundant in amorphous of β -iPP than α -iPP and this lack of stress transmitters create many weak interfaces between β -lamellae and facilitates the decoupling^{32-34, 37, 50, 51}. The applied stress initially exerted on the amorphous region between horizontal lamellae and resulted in the inter-lamellar slip, while the vertical lamellae were capable of taking more loads due to their higher modulus and is prone to deform at higher strain. Therefore, in the early stage of deformation, lamellar separation mainly occurred in the area where the lamellae were perpendicular to the loading direction, resulting in the formation of abundant slender deformation bands between β -lamellae (as marked with the letter A in Fig. 6a and b). Meanwhile, sporadic intra-lamellar slip was also spotted in the areas where the lamellae were parallel to the loading direction, leading to the formation of a few small crazes (as presented with the letter B in both PP-110 and PP-135). It also should be noted that owing to its thicker lamellae, PP-135 (shown in Fig. 6b) created larger cavities

compared with PP-110 (shown in Fig. 6a). Nevertheless, for both films, there were still some areas, which were composed of either greater spherulite (as marked with letter C) or flat-on β -lamellae (as marked with letter D), were too rigid to be deformed at yielding point.

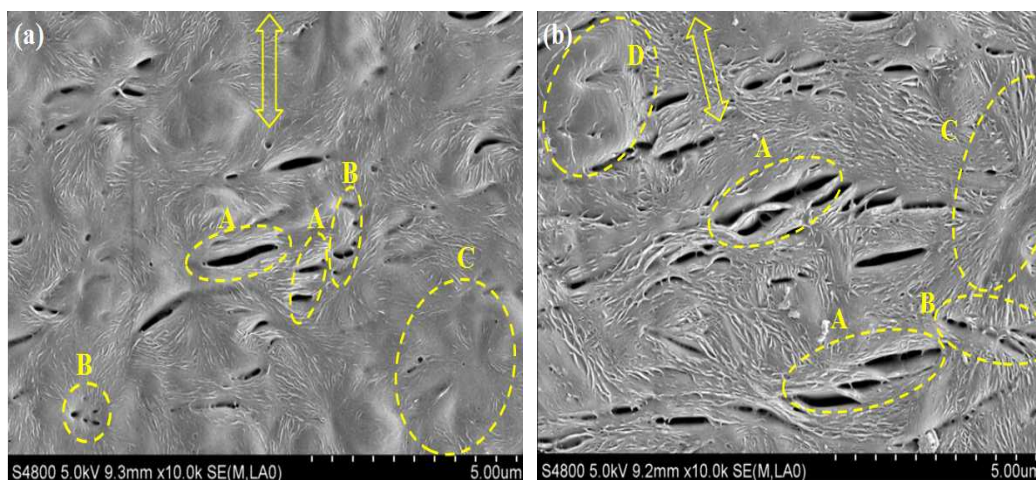


Fig. 6. SEM micrographs of β -PP samples stretched to $\varepsilon = 20\%$ at 25°C , $10000\times$: (a) PP-110 and (b) PP-135. The arrow indicates the loading direction.

As the strain increased to 50%, for both PP-110 and PP-135 samples, some deformation bands coalesced and developed into greater cracks after the yielding point (shown in Fig. 7). It is clear to see that numerous horizontal lamellae bundles slipped and separated, leading to the formation of large cracks (as marked with the letter A in Fig 7a and b). Meanwhile, the local stress concentration also induced distortions or even the disintegration of vertical lamellae, resulting in the formation of some small crazes as marked with the letter B. Furthermore, it is worth mentioning that there were still some rigid areas, which were mainly composed of flat-on lamellae (as marked with the letter C in Fig. 7b), could not be deformed^{33-35, 37}.

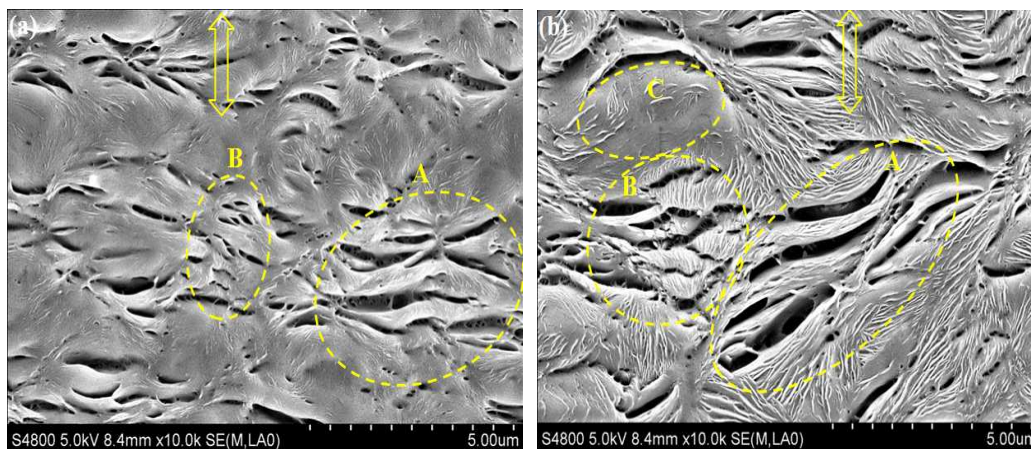


Fig. 7. SEM micrographs of β -PP samples stretched to $\epsilon = 50\%$ at $25\text{ }^\circ\text{C}$, $10000\times$: (a) PP-110 and (b) PP-135. The arrow indicates the loading direction.

Fig. 8 exhibits the morphologies of β -iPP samples with further deformation at $T_d=25\text{ }^\circ\text{C}$. When stretched to $\epsilon=100\%$, abundant deformation bands had been generated, and the lamellae broke up into fragments continually and tilted towards the loading direction, resulting in a substantial β -smectic transformation which has been proved by the previous WAXD results. Furthermore, it is clear to see that PP-135 (shown in Fig. 8b) had larger deformation bands compared with PP-110 (shown in Fig. 8a). Nevertheless, these cavities distributed unevenly in both membranes.

As the strain increased to $\epsilon=300\%$ (shown in Fig. 8c and d), fully developed crazes or cracks were observed, and some highly deformed lamellae were found bridging the two sides of crazes. The lamellar structure had converted into a highly oriented structure in the cold drawn membranes, which was consistent with the previous WAXD results in Fig. 4c and f that a strong diffraction peak appeared along the loading direction with a concomitant faint β (3 0 0) reflection. Furthermore, it is interesting to see that for PP-110 (shown in Fig. 8c) at high strain, the microfibrils were packed densely to decrease the porosity instead of forming new pores, which further verifies the porosity trend in Table 2 that it declined gradually when $\epsilon>200\%$. On the other hand, PP-135 whose lamellae were thicker and more stable could resist the lamellar deformation and volume contraction effectively, resulting in the maximal porosity value at even higher strain ($\epsilon=300\%$).

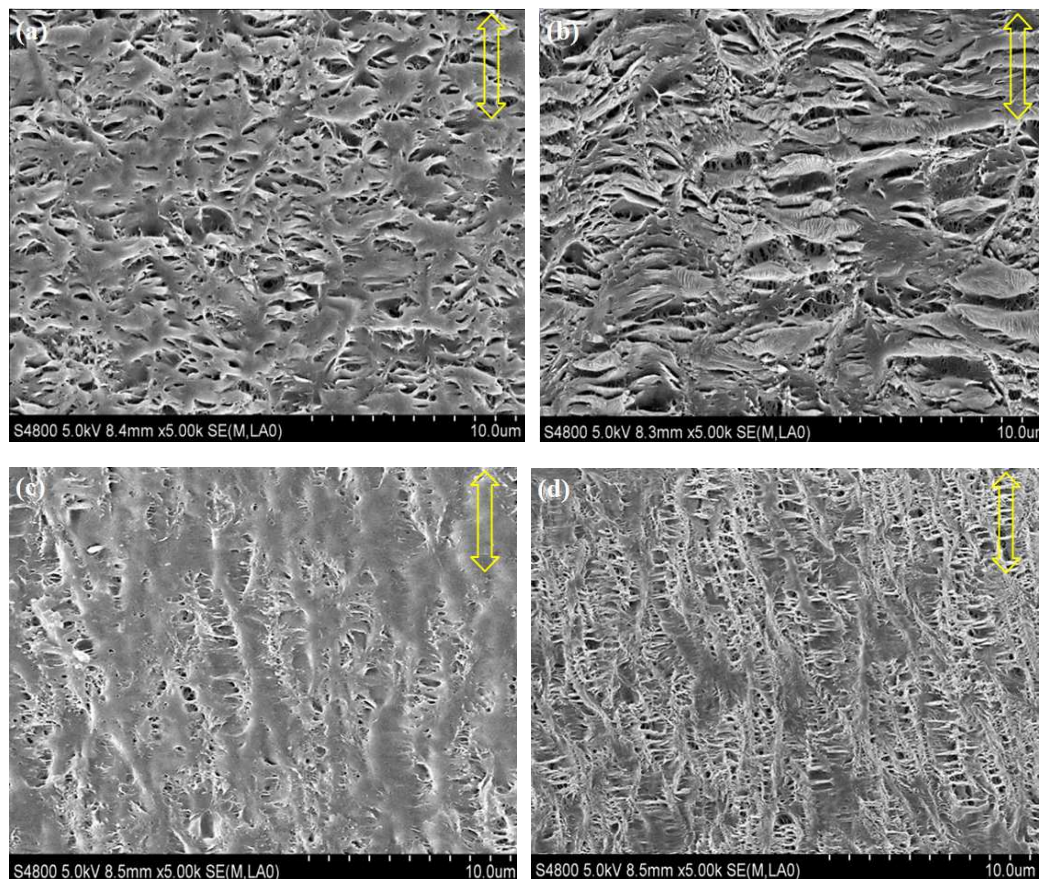


Fig. 8. SEM micrographs of β -PP samples stretched to $\varepsilon = 100\%$ and $\varepsilon = 300\%$ at 25°C , $5000\times$: (a) PP-110- $\varepsilon=100\%$; (b) PP-135- $\varepsilon=100\%$; (c) PP-110- $\varepsilon=300\%$; (d) PP-135- $\varepsilon=300\%$.

The arrow indicates the loading direction.

With the above considerations, it is concluded that the β -smectic transformation takes place during stretching at 25°C , and the micropores are directly induced at the weak interfaces between β -lamellae and enlarge with further deformation. Furthermore, the porosity is correlated to the lamellar thickness, namely the thicker lamellae facilitate the formation of higher porosity during cold drawing. In addition, the polydispersity of β -lamellae that have different angles to the tensile axis would lead to different deformational modes during stretching and thus result in the poor pore size distribution in stretching β -iPP membrane.

3.4.2 Stretching at 90°C

Microscopic lamellar deformation process of β -iPP when stretched at 90°C , where

the β - α transformation enters into action, is equally important to clarify the mechanism of pores formation and has never been investigated in detail before. Fig. 9 discloses the morphologies of PP-110 and PP-135 around yielding point ($\epsilon=20\%$) at 90°C under tensile loading, where no phase transformation was detected by WAXD (as is shown in Fig. 5). It is clear to see that there were still large amount of β -lamellae existing in both films and a great variety of deformation bands had been generated. However, these crazes distributed in all directions in the membranes, which were quite different from those formed at 25°C (shown in Fig. 9) that mainly concentrated along the horizontal direction. This is likely due to the promotion of the mobility of amorphous chains and lamellar movement when stretching at high temperature, and thus the rotation of β -lamellae is activated^{14-16, 20, 50}. For both films, substantial slender deformation bands were induced by the inter-lamellae slip between horizontal lamellae (as marked with the letter A) and those at a tilt angle to the loading direction (as marked with the letter D). Furthermore, sporadic tiny crazes were also originated from the intra-lamellar slip of vertical lamellae (as marked with the letter B). It is also worth mentioning that there were still some rigid areas in both membranes (as marked with the letter C) that could not be deformed at yielding point.

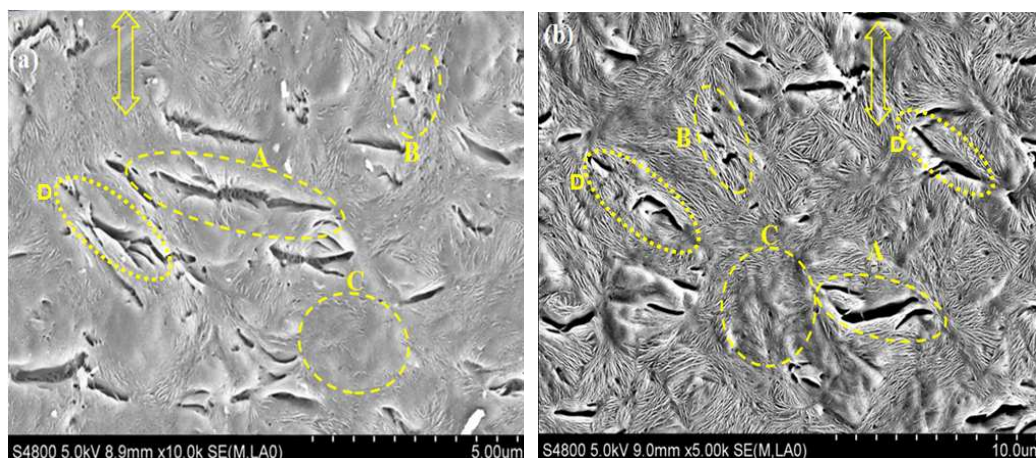


Fig. 9. SEM micrographs of β -PP samples stretched to $\epsilon = 20\%$ at 90°C , 10000 \times : (a) PP-110 and (b) PP-135. The arrow indicates the loading direction.

When the strain increased to 50%, where the β - α transformation took place progressively as proved by WAXD results in Fig. 5, the SEM micrographs of PP-110

and PP-135 (shown in Fig. 10) differed considerably. It is very interesting to note that only a few β -lamellae were observed in the PP-110 membrane accompanied by some shallow and small deformation bands (shown in Fig. 10a), indicating that large amount of β -crystal had transformed into α -crystal. However, as for PP-135 (shown in Fig. 10b), plenty of large deformation bands were created with substantial residual β -lamellae, implying that only partial of β -crystal had transformed into α -crystal, which was in accord with the previous WAXD results. Furthermore, the lamellae perpendicular to the loading direction underwent the phase transformation in an earlier stage of stretching, which would enlarge the pores (as marked with the letter A in Fig. 10b), because the stretching stress exerted on was along the molecular chains and allowed chain unfolding which facilitates β - α transformation. On the other hand, sporadic small crazes were also spotted (as marked with the letter B in Fig. 10b) due to the intra-lamellar slip of those parallel to the loading direction. These deformation bands could not grow much wider or develop into deformation network, for these β -lamellae have higher modulus and could not rotate towards the loading direction until the adjacent lamellae are stretched heavily, thus resulting in the residue of substantial vertical β -lamellae which packed densely^{17, 18, 31, 49}.

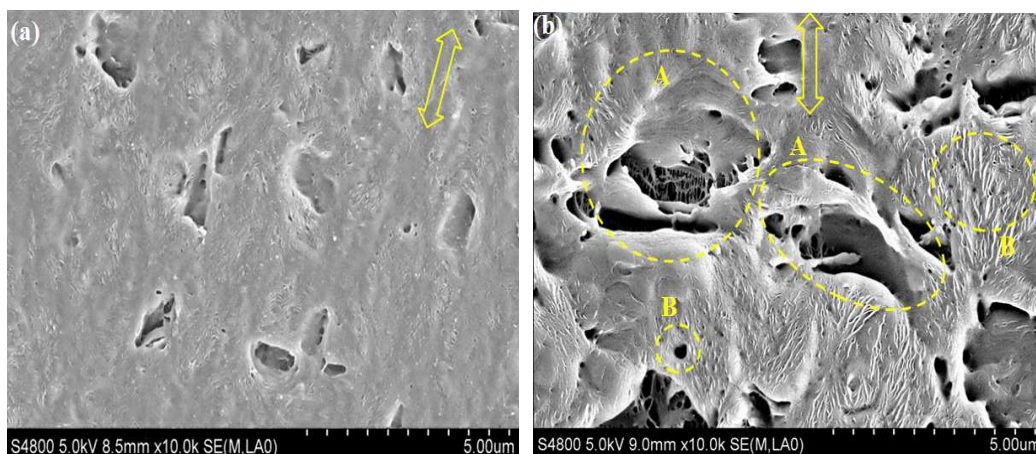


Fig. 10. SEM micrographs of β -PP samples stretched to $\epsilon = 20\%$ at 90°C , $10000\times$: (a) PP-110 and (b) PP-135. The arrow indicates the loading direction.

Fig. 11 shows the morphologies of β -iPP films with further deformation at 90°C . For PP-110 when stretched to $\epsilon=100\%$ (shown in Fig. 11a), some shallow deformation

bands were created along the loading direction without obvious β -lamellae, indicating that substantial β - α transformation had taken place. Furthermore, as the strain increased to 300%, only sporadic small crazes existed in PP-110 membranes. This phenomenon was likely to be induced by the continuous deformation of unstable β -lamellae and transformation into α -crystal, which would cause a serious volume contraction and hinder the microvoid formation. That is why PP-110 sample became translucent and had much lower porosity when stretched at 90 °C (as is shown in Fig. 3a and Table 2).

On the other hand, as for PP-135 when stretched to $\epsilon=100\%$ at 90 °C (shown in Fig. 11c), it is clear to see that the substantial crazes or cracks were enlarged with further deformation (as marked with the letter A). Moreover, a few tiny crazes (as marked with the letter B in Fig. 11c) which originated by intra-lamellar slip of the lamellae parallel to the tensile axis were also observed. In addition, there were still some rigid areas in which residual thinning vertical lamellae existed, for these lamellae could not move until the neighboring lamellar movement adds extra stress on them, therefore, they would pack more densely and the phase transformation is prone to occur at higher strain. On the other hand, as the stress exerted on is perpendicular to the molecular chains of vertical lamellae, the chain unfolding involving β - α transformation would lead to the formation of new α -crystals that pack together to prevent the growth of crazes. As the strain increased to 300% (shown in Fig. 11d), it is clear to see that the lamellar structure converted into an oriented fibril structure, where fully developed crazes were formed. However, these cavities distributed unevenly in the membranes: there were numerous highly oriented microfibrils and some rigid areas, as marked with the letter C in Fig. 11d, which might be difficult to be deformed during the transverse drawing. Since it is well established that the defects formed during uniaxial stretching are the precursors of pores after transverse stretching, these unevenly distributed deformation bands would result in the poor pore size distribution in the biaxial stretching β -iPP membrane.

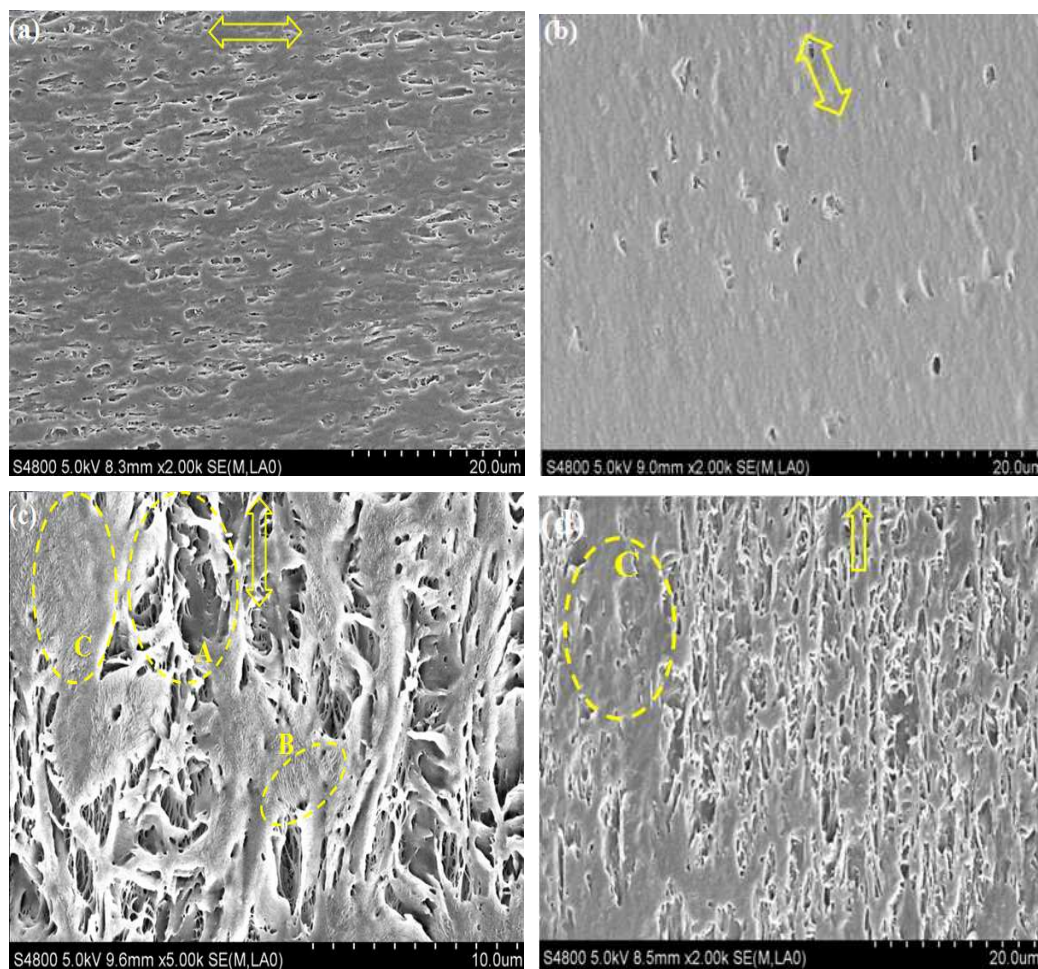


Fig. 11. SEM micrographs of β -PP samples stretched to $\varepsilon = 100\%$ and $\varepsilon = 300\%$ at $90\text{ }^{\circ}\text{C}$: (a) PP-110- $\varepsilon=100\%$, 2000 \times ; (b) PP-110- $\varepsilon=300\%$, 2000 \times ; (c) PP-135- $\varepsilon=100\%$, 5000 \times ; (d) PP-135- $\varepsilon=300\%$, 2000 \times . The arrow indicates the loading direction.

Based on the above considerations, the morphological differences between PP-110 and PP-135 during stretching at $90\text{ }^{\circ}\text{C}$ mainly depend on the stability of β -crystals. The β -lamellae formed at $T_c = 110\text{ }^{\circ}\text{C}$ are easier to deform and undergo a rapid β - α transformation, resulting in a marked volume contraction which decreases the porosity dramatically. On the other hand, the β -lamellae formed at $T_c = 135\text{ }^{\circ}\text{C}$ are more stable and could resist the crystal transformation efficiently, hence, the stretching stress would concentrate on the pores' boundaries and enlarge the pores rather than that expected from the volume contraction^{14-16, 19-21}.

3.5. Pores formation mechanism of stretching β -iPP and modification strategy

Together with the previous discussions, it is concluded that the phase transformation of β -smectic (at $T_d=25$ °C) and β - α (at $T_d=90$ °C) are not the primary origin of pore formation in stretching β -iPP, instead, the micropores are directly induced due to the abundant weak interfaces between β -lamellae. As has been examined by SEM in Fig. 2, the β -iPP samples we prepared were composed of bundle-like lamellar blocks surrounded by substantial weak areas of amorphous phase, which increase the tendency for β -iPP to cavitate during stretching relative to α -iPP whose mobility of the amorphous phase is restricted by cross-hatched structures^{36, 41, 48}. Therefore, it is reasonable to understand the strange phenomena that stretching at 25 °C, in which β -smectic phase transformation was predominant, induced a higher porosity than stretching at 90 °C, in which β - α phase transformation was activated, and a large number of microvoids had formed at very low strain without obvious phase transformation. Furthermore, we postulate a detailed model, involving the morphological evolutions and phase transformation processes during stretching at different temperatures, to explain the mechanism of microvoids formation in stretching β -iPP (shown in Fig. 12a).

In the case of stretching at 25 °C, where β -smectic transformation are predominant^{8, 21, 22, 30}, three primary deformation modes have been proposed in the studies of Li³²⁻³⁵ and Lezak³⁰, namely (1) separation of lamellae, (2) inter-lamellar slip and (3) intra-lamella slip. Separation of horizontal lamellae is a main mode in the early stage of deformation. After yielding point, intra-lamellar slip is activated in the areas where the lamellae are along the loading direction, resulting in the local distortion and disintegration of vertical lamellae. Meanwhile, inter-lamellar slip is likely to occur in the lamellae perpendicular to the loading direction. In this present work, however, we found that the amorphous chains of β -iPP have comparable modulus to the β -lamellae when stretching at low temperature, thus the rotation of β -lamellae towards the loading direction is retarded, resulting in the existence of an intact β (3 0 0) ring in 2D-WAXD results during the whole stages of deformation (seen in Fig. 4). Furthermore, substantial crazes, which mainly distribute in the

horizontal direction, have formed in the early stage of deformation. Inter-lamellar slip of lamellae perpendicular to the loading direction would lead to the formation of great crazes or cracks between lamellae, which could be enlarged or even combine with continuous deformation. On the other hand, sporadic small crazes are also created by intra-lamellar slip of lamellae whose c axis tilting to the drawing direction. In this case, the crazes cannot grow much wider or develop into deformation network, for the lamellae at a tilt angle to the tensile axis, which could not move until the adjacent lamellae are stretched heavily, are likely to undergo the β -smectic transformation at larger strain and would pack more densely to form the compact regions with further deformation. At high strain, these fragmented β -lamellae would flow towards the loading direction and consequently lead to the formation of c-axis oriented smectic phase.

In the case of stretching at 90 °C, in which β - α transformation enters into action, partial rotation of β -lamellae along the tensile axis is allowed due to the promotion of the mobility of amorphous chains and lamellar movement^{14-16, 20, 50}. At the early stage of deformation, the horizontal lamellae and those at a tilt angle to the loading direction separate and form slender crazes which could be enlarged or even collapsed with excessive deformation. On the other hand, sporadic intra-lamellar slip which leads to the formation of small crazes is also observed for vertical lamellae. As for the lamellae with c axis perpendicular to the drawing directions, lamellar rotation may be retarded because the stretching stresses exerted on are from the four directions and counteract each other, consequently, these lamellae would become thinner and pack more densely and the phase transformation is likely to be activated at higher strain. In addition, the newly born α -crystal would pack together to form the rigid areas which is difficult to be deformed during transverse stretching. Furthermore, the stability of β -lamellae is critical to determine the porosity of β -iPP membranes: if the β -crystal is not stable (such as PP-110), the β -lamellae would rapidly fragment and transform into α phase, leading to a marked volume shrinkage and consequent decrease of porosity and pore size. On the contrary, if the β -lamellae are stable enough (such as PP-135), the phase transformation would undergo at a lower rate and the stretching stress

would concentrate on the pores' boundaries and enlarge the pores rather than that expected from the volume contraction. As a conclusion, the bundle-like β -lamella without fully developed spherulites, is an asymmetric three dimensional structure. The lamellae at different angles to the tensile axis would result in different deformational modes and lead to the formation of unevenly distributed crazes during stretching, and consequently cause the poor pore size distribution in the final membrane after transverse stretching.

Since we have established that the less stable β -lamellae would lead to the marked volume shrinkage and thus deteriorate the porosity, we improved our fabrication process by fixing the two other free sides of β -iPP films during stretching, which could resist the shrinkage efficiently. Fig. 12b shows the photographs of M-PP-110 after uniaxial stretching to $\epsilon=100\%$ and $\epsilon=300\%$ at $90\text{ }^\circ\text{C}$ with constant width, it is very interesting to see that these membranes were completely opaque, indicating the formation of abundant microvoids during these processes. Furthermore, the cross section and surface images of M-PP-110 and M-PP-135 after biaxial stretching with constant width are also displayed in Fig. 12c-f. It is clear to see from the cross section views that a large number of micropores had formed in these two membranes (shown in Fig. 12c and d). The porosity of M-PP-110 (40.6%) and M-PP-135 (49.8%) had improved dramatically. Moreover, the surface images (shown in Fig. 12e and f) also exhibit that the porosity and pore size of both membranes increased significantly compared with those stretched with free width (seen in Fig. 3e and f). These results further support the pores formation mechanism of stretching β -iPP we propose above. However, owing to the polydispersity of lamellae in β -iPP, the pore size distribution were still poorer when compared with those produced through "dry uniaxial stretch"³⁻⁵ and "wet biaxial stretch"¹⁰ methods, resulting in the limitation of its applications in high tech fields. Therefore, we suggest that fabrication of anisotropic oriented β -iPP precursor films with all the lamellae growing along the same direction, which we are still working on, would be a practical solution.

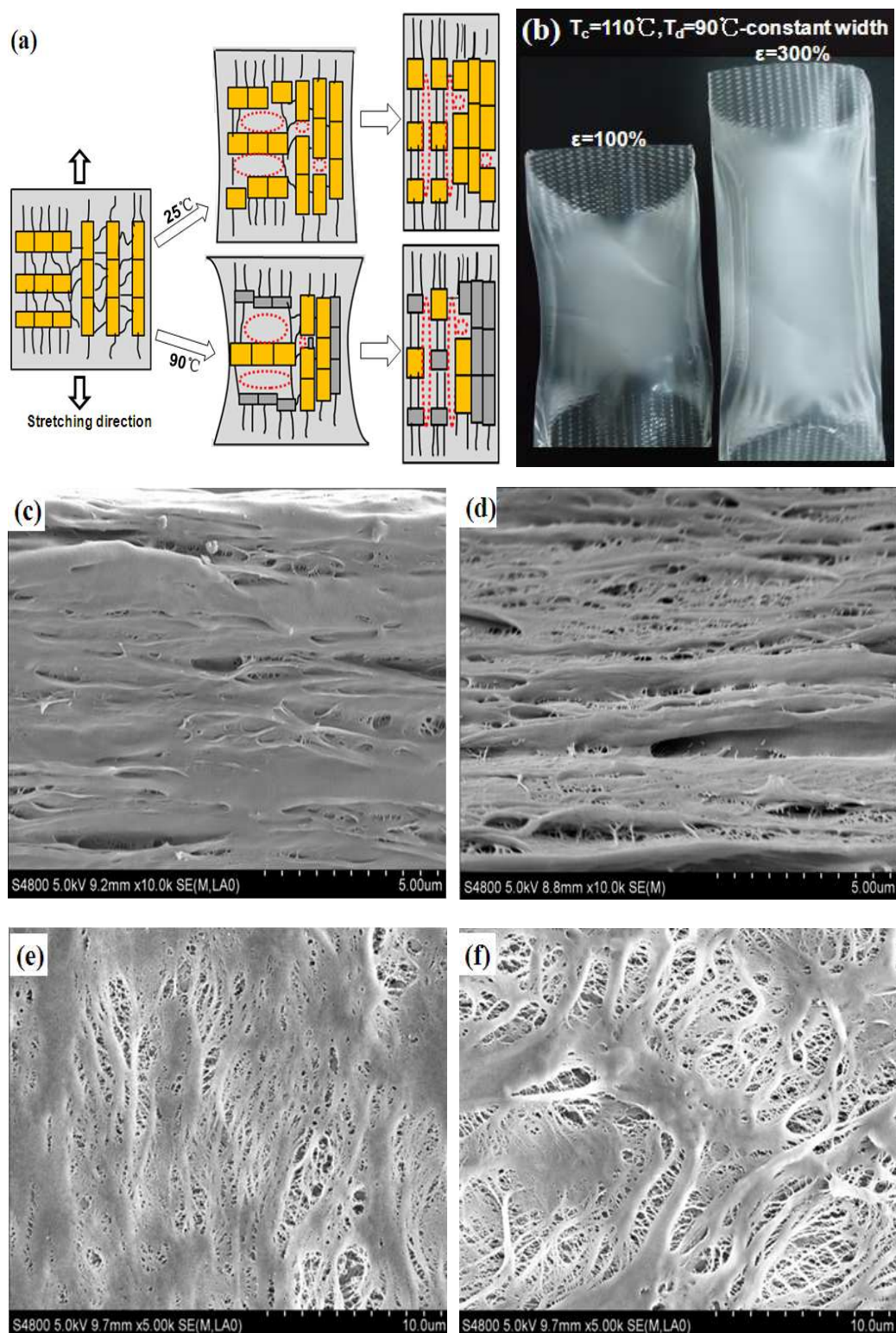


Fig. 12. (a) Schematic diagram of pores formation mechanism of β -PP during stretching at 25°C and 90°C ; (b) Photographs of M-PP-110 after uniaxially stretched to $\epsilon=100\%$ and $\epsilon=300\%$ with constant width at 90°C ; cross section images of biaxially stretched films with

constant width: (c) M-PP-110 and (d) M-PP-135, 10000 \times ; and surface images: (e) M-PP-110 and (f) M-PP-135, 5000 \times .

4. Conclusions

In this article, two β -iPP films were prepared through crystallizing at 110 $^{\circ}\text{C}$ and 135 $^{\circ}\text{C}$. The DSC, WAXD and SEM results show that the two cast films, which were composed of bundle-like lamellae, had almost the same crystallinity and high contents of β -crystal. Then uniaxial and biaxial stretching was performed at different temperatures. The 2D-WAXD results suggest that β phase transformed into smectic phase at 25 $^{\circ}\text{C}$, while β - α transformation entered into action when stretched at 90 $^{\circ}\text{C}$. Furthermore, the β -crystal formed at 110 $^{\circ}\text{C}$ was less stable and underwent the β -smectic or β - α transformation more quickly than those formed at 135 $^{\circ}\text{C}$. On the other hand, the morphological evolutions of β -iPP during stretching were investigated by SEM measurements in details. We found that the phase transformation of β -smectic and β - α are not the primary origin of pore formation in stretching β -iPP, instead, the micropores are directly created at the weak areas or interfaces between β -lamellae and enlarge with further deformation. Moreover, the polydispersity of lamellae in β -iPP is the root cause leading to the poor pore size distribution in stretching β -iPP membrane. In addition, we modified the fabrication condition by stretching with constant width, which could hinder the volume contraction efficiently and improve the porosity of β -iPP membranes significantly.

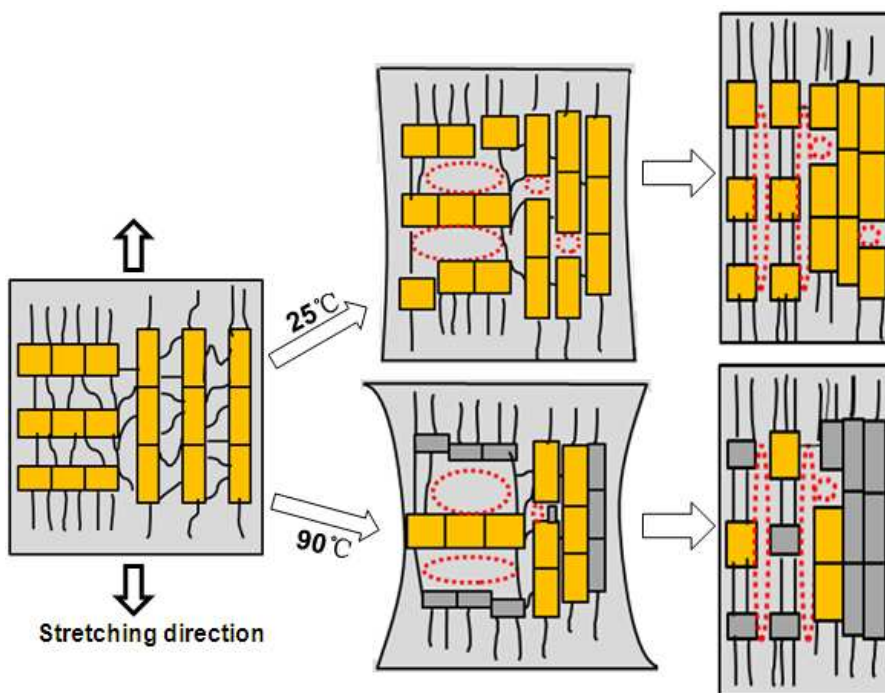
References

1. B. S. Lalia, V. Kochkodan, R. Hashaikeh and N. Hilal, *Desalination*, 2013, 326, 77-95.
2. P. Arora and Z. Zhang, *Chem. Rev.*, 2004, 104, 4419-4462.
3. H. S. Bierenbaum, R. B. Isaacson, M. L. Druin and S. G. Plovon, *Ind. Eng. Chem. Prod. Res. Dev.*, 1974, 13, 2-9.
4. F. Sadeghi, A. Ajji and P. J. Carreau, *Journal of Membrane Science*, 2007, 292, 62-71.
5. S. H. Tabatabaei, P. J. Carreau and A. Ajji, *Journal of Membrane Science*, 2008, 325, 772-782.
6. S. H. Tabatabaei, P. J. Carreau and A. Ajji, *Polymer*, 2009, 50, 4228-4240.
7. *U.S. Patent Pat.*, 6,368,742, 2002.
8. *U.S. Patent Pat.*, 5,134,174, 1992.
9. *U.S. Patent Pat.*, 5,317,035, 1994.

10. S. S. Kim and D. R. Lloyd, *Journal of Membrane Science*, 1991, 64, 13-19.
11. S. J. Liu, C. X. Zhou and W. Yu, *Journal of Membrane Science*, 2011, 379, 268-278.
12. *U.S. Patent Pat.*, 4,620,956, 1986.
13. *U.S. Patent Pat.*, 5,691,047, , 1997.
14. F. Chu, T. Yamaoka, H. Ide and Y. Kimura, *Polymer*, 1994, 35, 3442-3448.
15. F. Chu, T. Yamaoka and Y. Kimura, *Polymer*, 1995, 36, 2523-2530.
16. F. Chu, *Polymer*, 1996, 37, 573-579.
17. G. T. Offord, S. R. Armstrong, B. D. Freeman, E. Baer, A. Hiltner and D. R. Paul, *Polymer*, 2013, 54, 2796-2807.
18. G. T. Offord, S. R. Armstrong, B. D. Freeman, E. Baer, A. Hiltner, J. S. Swinnea and D. R. Paul, *Polymer*, 2013, 54, 2577-2589.
19. S. Ran and M. Xu, *Chinese Journal of Polymer Science*, 2004, 22, 123-130.
20. S. Ran, X. Zong, D. Fang, B. S. Hsiao and B. Chu, *Macromolecules*, 2001, 34, 2569-2578.
21. G. Shi, F. Chu, G. Zhou and Z. Hang, *Makromol. Chem*, 1989, 190, 907-913.
22. W. Zhu and M. Xu, *Polymers for Advanced Technologies*, 1996, 7, 743-748.
23. A. T. Jones, J. M. Aizlewood and D. R. Beckett, *Die Makromolekulare Chemie*, 1964, 75, 134-158.
24. G. Natta and P. Corradini, *Del Nuovo Cimento* 1960, 15, 40-51.
25. J. Kang;, G. S. Weng;, Z. F. Chen;, J. Y. Chen;, Y. Cao;, F. Yang; and M. Xiang, *RSC Advances*, 2014, 4, 29514 - 29526.
26. S. V. Meille, D. R. Ferro, S. Brueckner, A. J. Lovinger and F. J. Padden, *Macromolecules*, 1994, 27, 2615-2622.
27. B. Lotz, J. C. Wittmann and A. J. Lovinger, *Polymer*, 1996, 37, 4979-4992.
28. W. Stocker, M. Schumacher, S. Graff, A. Thierry, J. C. Wittmann and B. Lotz, *Macromolecules* 1998, 31, 807-814.
29. E. Lezak and Z. Bartczak, *Journal of Polymer Science: Part B: Polymer Physics* 2008, 46, 92-108.
30. E. Lezak, Z. Bartczak and A. Galeski, *Polymer*, 2006, 47, 8562-8574.
31. S. R. Armstrong, G. T. Offord, D. R. Paul, B. D. Freeman, A. Hiltner and E. Baer, *Journal of Applied Polymer Science*, 2014, 131.
32. J. X. Li and W. L. Cheung, *Journal of Applied Polymer Science*, 1999, 72, 1529-1538.
33. J. X. Li, W. L. Cheung and C. M. Chan, *Polymer*, 1999, 40, 2089-2102.
34. J. X. Li, W. L. Cheung and C. M. Chan, *Polymer*, 1999, 40, 3641-3656.
35. J. X. Li and W. L. Cheung, *Polymer*, 1998, 39, 6953-6940.
36. R. A. Phillips and M. D. Wolkowicz, *Polypropylene Handbook*, Hanser Gardner Publications, Inc., OH, USA, 2005.
37. J. Varga, *Journal of Macromolecular Science, Part B-Physics*, 2002, 41 1121-1171.
38. H. Huo, S. C. Jiang and L. J. An, *macromolecules*, 2004, 37, 2478-2483.
39. F. Luo, C. Geng, K. Wang, H. Deng, F. Chen, Q. Fu and B. Na, *macromolecules*, 2009, 42, 9325-9331.
40. R. H. Olley and D. C. Bassett, *Polymer*, 1982, 23, 1707-1710.
41. S. Bruckner and S. V. Meille, *Polypropylene*, Kluwer Academic Publishers, Dordrecht, The Netherlands, 1999.
42. Q. Lu and Q. Dou, *Journal of Polymer Research*, 2009, 16, 555-560.

43. J. Kang, J. Gai, J. Li, S. Chen, H. Peng, B. Wang, Y. Cao, H. Li, J. Chen, F. Yang and M. Xiang, *Journal of Polymer Research*, 2013, 20.
44. J. Kang, Z. Chen, T. Zhou, F. Yang, J. Chen, Y. Cao and M. Xiang, *Journal of Polymer Research*, 2014,, 21.
45. J. Varga, I. Mudra and G. W. Ehrenstein, *Journal of Applied Polymer Science*, 1999, 74, 2357-2368.
46. J. Varga, I. Mudra and G. W. Ehrenstein, *Journal of Thermal Analysis and Calorimetry*, 1999, 56, 1047-1057.
47. C. Grein, *Advances in Polymer Science*, 2005, 188, 43-104.
48. T. Wu, Y. Cao, F. Yang and M. Xiang, *Materials & Design*, 2014, 60, 153–163.
49. R. Y. Bao, Z. T. Ding, Z. Y. Liu, W. Yang, B. W. Xie and M. B. Yang, *Polymer*, 2013, 54, 1259-1268.
50. H. W. Bai, F. Luo, T. N. Zhou, H. Deng, K. Wang and Q. Fu, *Polymer*, 2011, 52, 2351-2360.
51. C. Grein, C. J. G. Plummer, H. H. Kausch, Y. Germain and P. Beguelin, *Polymer*, 2002, 43, 3279-3293.

Graphical Abstract



Schematic diagram of pores formation mechanism of β -PP during stretching at 25°C and 90°C